Catalytic Activities of Subnanometer Gold Clusters ($Au_{16}-Au_{18}$, Au_{20}, and $Au_{27}-Au_{35}$) for CO Oxidation

Yi Gao,[†] Nan Shao,[‡] Yong Pei,[§] Zhongfang Chen,[⊥] and Xiao Cheng Zeng[†,*]

[†]Department of Chemistry, University of Nebraska—Lincoln, Lincoln, Nebraska 68588, United States, [‡]Chemical Sciences Division, Oak Ridge National Laboratory, Oak Ridge, Tennessee 37831, United States, [§]Department of Chemistry, Xiangtan University, Hunan Province, China 411105, and [⊥]Department of Chemistry, University of Puerto Rico, San Juan, Puerto Rico 00931

ABSTRACT Using the CO oxidation as a chemical probe, we perform a comprehensive *ab initio* study of catalytic activities of subnanometer gold clusters. Particular attention is placed on 12 different clusters in the size range of $Au_{16}-Au_{35}$, whose atomic structures in the anionic state have been resolved from previous experiments. Adsorption energies of a single CO or O_2 molecule as well as coadsorption energies of both CO and O_2 molecules on various distinctive surface sites of each anionic cluster and their neutral counterpart are computed. In general, the anionic clusters can adsorb CO and O_2 more strongly than their neutral counterparts. The coadsorption energies of both CO and O_2 molecules decrease as the size of gold clusters increases with the exception of Au_{34} (an electronic "magic-number" cluster). Besides the known factor of low coordination site, we find that a relatively small cone angle (<110°) associated with each surface site is another key geometric factor that can enhance the binding strength of CO and O_2. For the subnanometer clusters, although the size effect can be important to the strength of CO adsorption, it is less important to the activation energy. Using Au_{34} as a prototype model, we show that strong CO and O_2 adsorption sites tend to yield a lower reaction barrier for the CO oxidation, but they have little effect on the stability of the reaction intermediate. Our calculations support the notion that CO and O_2 adsorption energies on the gold clusters can be an effective indicator to assess catalytic activities of subnanometer gold clusters. This systematic study of the site- and size-dependent adsorption energies and reaction pathways enables a quantitative assessment of the site-size-activity relationship for the CO oxidation on subnanometer gold clusters.

KEYWORDS: subnanometer gold clusters · CO oxidation · site-dependent catalytic activities · site-by-site adsorption energies · density functional theory

Since the discovery of extraordinary catalytic activities of gold nanoparticles (AuNPs),[1−5] considerable efforts have been devoted to the investigation of important factors that contribute to their high catalytic activities.[6−23] These factors include the dimensionality and morphology of AuNPs,[18−20] the fluxionality and electronic state of the gold clusters,[13−17,24−26] the specific active sites on the gold clusters,[6,7] and the type and structure of oxide supports.[22−25] Nevertheless, the dominant factors are still not fully resolved due in part to the lack of experimental measurements of exact atomic structures of AuNPs,[7−10] particularly for the supported AuNPs.[27,28] On the other hand, with joint efforts by experimental and theoretical scientists, precise atomic structures of small gold clusters in the range of 3−20 gold atoms have been fully determined and confirmed over the past decade.[29−40] The acquired knowledge of precise structures of small-sized gold clusters has inspired numerous studies of their catalytic activities, either in the gas phase or on different oxide support.[24−26,41−52] Landman and co-workers carried out combined experimental and theoretical studies of the CO oxidation on size-selected small gold clusters supported by magnesia. Their study revealed that the supported Au_8 cluster is highly active for CO oxidation.[24,25] Nørskov and co-workers used Au_{10} cluster as a model system and predicted that Au_{10} can be highly active for the CO oxidation both in the gas phase[26] and on the rutile TiO_2 support.[30] Molina and Hammer performed a quantum-chemical study of the CO oxidation on three different gold clusters, Au_{15}, Au_{21}, and Au_{34}, supported by MgO and TiO_2, respectively.[43−45] They found that Au_{20} not only is a good catalyst for CO oxidation but also can become even more active if doped with a Na atom.[45] Bernhardt and co-workers revealed the full reaction cycle of CO oxidation on Au_2 and Au_3 by combining reaction kinetics measurements with *ab initio* calculations.[46−48]

Although impressive progress has been achieved on understanding catalytic activities of small-sized gold clusters, both in the gas phase and on the oxide support, theoretical studies of medium-sized to large-sized gold clusters are scarce due largely to limited information about precise atomic structures of gold clusters Au_N beyond the size $N = 20$. Without this information, the structure-activity-selectivity relationship for gold-cluster-catalyzed reactions, either on the oxide support or in the gas phase, cannot be quantitatively characterized. Recently, atomic

* Address correspondence to xzeng1@unl.edu.

Received for review May 18, 2011 and accepted September 3, 2011.

Published online September 03, 2011
10.1021/nn201817b

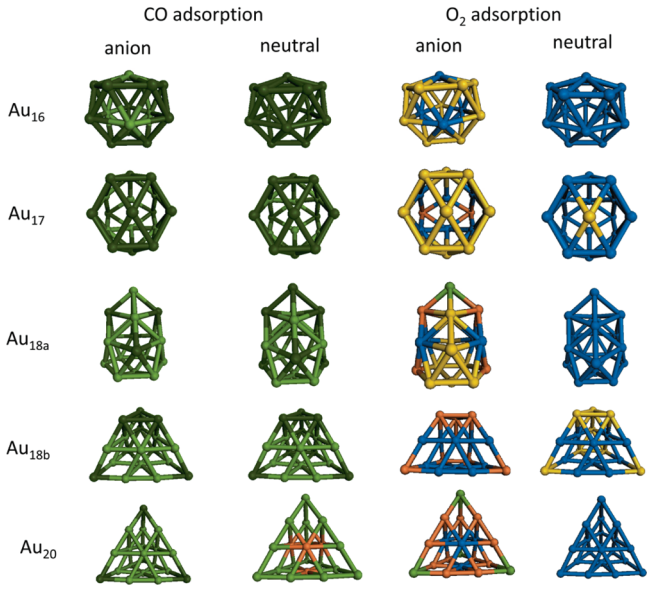

Figure 1. Schematic illustration of adsorption energies of CO and O_2 on anionic and neutral clusters Au_{16}−Au_{18}, and Au_{20}. Adsorption energy color code: dark green, <−0.9 eV; green, −0.5 to −0.9 eV; orange, −0.2 to −0.5 eV; gold yellow, 0.0 to −0.2 eV; blue, no binding. Negative sign represents exothermic process in adsorption.

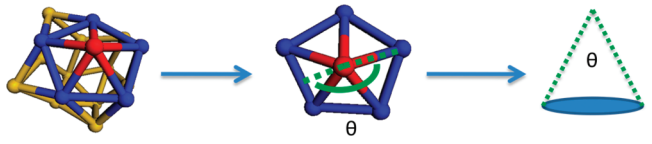

Scheme 1. Definition of the cone angle θ for a surface site (red), which is constructed based on the central surface site (red) and one of nearest-neighbor sites, and a midpoint on the opposing bond (connected by green dashed line). Although this angle is dependent on the chosen nearest-neighbor site, its variance is typically less than 5° from the average value.

structures of several subnanometer to 1 nm anionic gold clusters Au_N^- in the size range of N = 27−35 (excluding N = 29 and 31 due to presence of multiple nearly isoenergetic isomers for these two sizes) and N = 55−64 have been determined through joint experimental measurements and quantum-chemical calculations.[53−56] In this article, we report a systematic study of site-dependent adsorption energies, reaction pathway, and reaction barriers for the CO oxidation on anionic gold clusters of Au_{16}−Au_{18},[30,36,38,40] Au_{20},[33,37] Au_{27},[56] Au_{28},[56] Au_{30},[56] Au_{32}−Au_{35}[56] (see Figures 1−3), and their neutral counterparts. The atomic structures of these clusters in the anionic state have been determined through joint anion photoelectron spectroscopy experiment and density functional theory calculation.[56] To our knowledge, this is the first comprehensive quantum-chemical study, in a site-by-site and atom-by-atom fashion, of catalytic activities of subnanometer gold clusters. This study can provide additional insights, at the atomic level, into the site-size-activity relationship for the subnanometer gold clusters. Note that in this paper our focus is placed on the free-standing gold clusters in the gas phase. Even with the same structures, their catalytic activities are likely different from the gas phase when placed on an oxide support. The support effect will be investigated in the future.

RESULTS AND DISCUSSION

CO and O_2 Adsorption Energies. We first examine every distinctive site of anionic gold clusters and their neutral counterparts for CO and O_2 adsorption. As a result, we have generated a large database of CO and O_2 adsorption energies associated with every surface site of the 12 gold clusters: Au_{16}−Au_{20}, Au_{27}, Au_{28}, Au_{30}, and Au_{32}−Au_{35}.

Au_{16}−Au_{20} (Hollow Cages to Pyramids). The calculated adsorption energies of CO and O_2 on anionic and neutral Au_{16}−Au_{18} and Au_{20} clusters are schematically illustrated in Figure 1, where different colors are used to describe the binding capability of every surface site on these clusters. Dark green represents relatively strong exothermic adsorption (adsorption energies <−0.9 eV); green represents moderate exothermic adsorption (adsorption energies are between −0.5 and −0.9 eV); orange represents relatively weak exothermic adsorption (adsorption energies are between −0.2 and −0.5 eV); golden yellow represents very weak exothermic adsorption (adsorption energies are between 0 and −0.2 eV); and blue represents no exothermic adsorption at all. As shown in Figure 1,

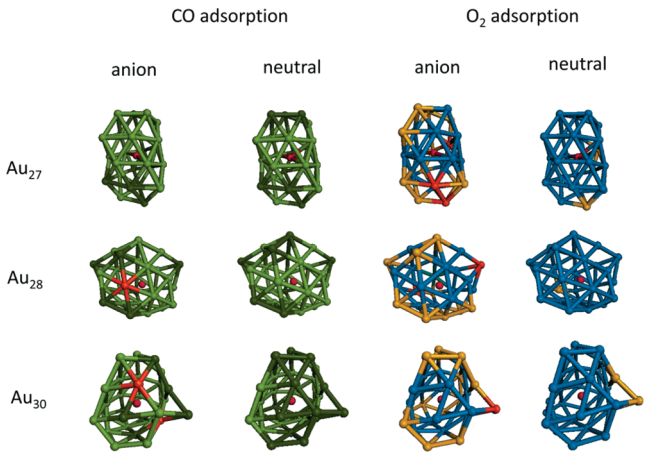

Figure 2. Schematic illustration of adsorption energies of CO and O_2 on anionic and neutral clusters Au_{27}, Au_{28}, and Au_{30}. The single atom in the core is highlighted by a red sphere. Adsorption energy color code: dark green, <−0.9 eV; green ,−0.5 to −0.9 eV; orange, −0.2 to −0.5 eV; gold yellow, 0.0 to −0.2 eV; blue, no binding. Negative sign represents exothermic process in adsorption.

the CO adsorption is much stronger than the O_2 adsorption on both anionic and neutral clusters. In addition, we find that (1) although CO could be adsorbed on these gold clusters, the CO adsorption is stronger on the neutral Au_{16} and Au_{18} than on the anionic Au_{16}^- and Au_{18}^-, whereas the CO adsorption is stronger on the anion Au_{20}^- than the neutral Au_{20}. For Au_{17}, the anionic and neutral clusters give nearly the same CO adsorption energies. (2) Neutral Au_{16}, Au_{17}, Au_{18a}, and Au_{20} cannot adsorb O_2 (as illustrated by blue color in Figure 1), but several corner sites of neutral Au_{18b} can weakly and exothermically adsorb O_2 (with adsorption energy between 0 and −0.20 eV). (3) All anionic clusters adsorb O_2 more strongly than their neutral counterparts. On Au_{16}^-, only a few sites can adsorb O_2, albeit weakly; Au_{17}^- can adsorb O_2 on a few sites with adsorption energy up to −0.22 eV. O_2 adsorptions on Au_{18a}^- and Au_{18b}^- are stronger than those on Au_{16}^- and Au_{17}^-, with the adsorption energy of −0.50 and −0.38 eV, respectively. Finally, the O_2 adsorption on the corner sites of pyramidal Au_{20}^- is the strongest among Au_{16}^- to Au_{20}^-. In summary, from Au_{16} to Au_{20}, CO adsorption becomes weaker for both anionic and neutral species, while the O_2 adsorption becomes stronger for the anionic species.

To understand the correlation between local surface structure (and "active site") and the corresponding CO or O_2 adsorption energies for the gold clusters, we view that any Au atom on the surface of a cluster is surrounded by several nearest-neighbor Au atoms to form a cone-like structure, as depicted in Scheme 1, where the cone angle θ is defined by the angle between one bond and the midpoint of the opposing bond. Although there can be slight changes when different bonds stemming from the vertex point are chosen, the variation of θ is less than 5°, which is much smaller than the typical value of θ considered here. A reason we choose θ as another geometric indicator to determine each Au site's reactivity is that, in certain gold clusters, the Au−Au bond length can be within a range from 2.8 to 3.3 Å (for bulk gold or gold surface, the Au−Au bond length is within a very narrow range). So for gold clusters, the coordination number may be sensitive to the cutoff bond length defined. In certain cases, the sites with same coordination number can give different adsorption energy and activation energy barrier (see below). Thus, θ appears to be an additional indicator to identify site reactivity.

First, we consider the hollow cage Au_{16}^- whose surface sites are all strong CO binding sites. As shown in Figure 1, there are four surface sites that adsorb CO less strongly than other surface sites. A careful inspection of the four sites indicates that (1) each of the four surface sites is *six-coordinated*, while other sites that can adsorb CO more strongly are all *five-coordinated*. (2) The cone angle θ of all *six-coordinated* sites is about 150° (symmetric structure), while θ of those *five-coordinated* sites is much smaller, ranging from 90 to 100°.

Second, on the Au_{17}^- cage, there are six sites that adsorb CO weakly, while the remaining 11 sites adsorb CO more strongly. The former six sites are either five- or six-coordinated, while the remaining 11 sites are either four- or five-coordinated (Figure 1). Moreover, all the cone angles of the six sites are between 130 and 145°, while those of the 11 sites are between 90 and 100°, which accounts for these 11 relatively strong CO binding sites. In fact, four relatively weak CO binding sites cannot even adsorb the O_2 molecule, while those relatively strong CO binding sites can adsorb O_2 molecules, albeit weakly (see Figure 1).

Third, it is known that Au_{18}^- possesses two stable isomers with nearly degenerate energies.[38] One, Au_{18a}^-, exhibits a cage-like structure, and another, Au_{18b}^-, exhibits a truncated pyramidal structure. Both isomers can adsorb CO, albeit more weakly compared

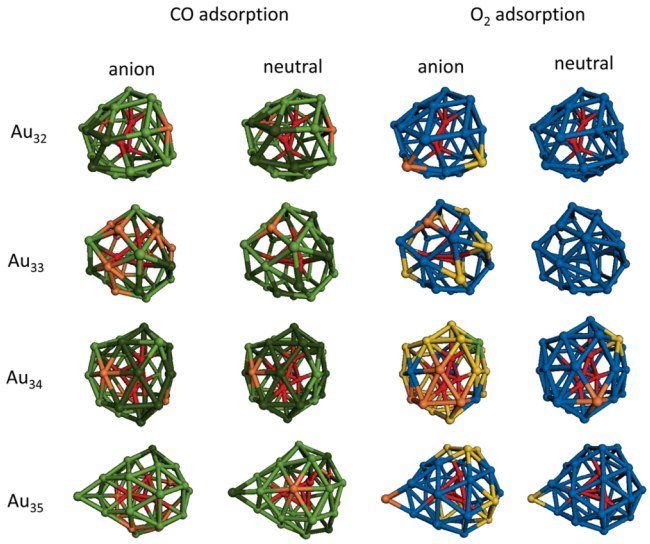

Figure 3. Schematic illustration of adsorption energies of CO and O_2 on anionic and neutral clusters Au_{32}−Au_{35}. Atoms in the core are highlighted by red spheres. Adsorption energy color code: dark green, <−0.9 eV; green, −0.5 to −0.9 eV; orange, −0.2 to −0.5 eV; gold yellow, 0.0 to −0.2 eV; blue, no binding. Negative sign represents exothermic process in adsorption. Adsorption energies of CO and O_2 on neutral icosahedral cage isomer of Au_{32} are illustrated in Supporting Information Figure S1.

to Au_{16} and Au_{17} in either anionic or neutral form. On the other hand, Au_{18a}^- is quite favorable for O_2 adsorption with the exothermic energy amounting to −0.50 eV, while Au_{18b}^- can also adsorb O_2 with the exothermic energy amounting to −0.38 eV. Both isomers can bind with O_2 much more strongly than with Au_{16} and Au_{17}, especially for the anionic species. The relatively strong CO binding sites of Au_{18a}^- are either five- or six-coordinated with the cone angle $\theta \sim 98-100°$, while those relatively weak CO binding sites of Au_{18a}^- are all six-coordinated with $\theta \sim 130-160°$.

Lastly, Au_{20} is a special case as the anionic Au_{20}^- can adsorb CO more strongly than the neutral Au_{20}. This unusual case may be attributed to the ultrahigh stability of the "magic-number" cluster Au_{20} with a very large HOMO−LUMO gap of 1.77 eV.[37] The extra electron of Au_{20}^- can be more easily donated to the $2\pi^*$ orbital of CO, thereby enhancing the binding between Au_{20}^- and CO. On the basis of the Hirshfeld charge analysis, Au_{20}^- donates 0.088e to CO, larger than the charge donated by Au_{16}^- (0.057e), Au_{17}^- (0.063e), and Au_{18b}^- (0.071e). Also, Au_{20}^- can donate as much as 0.39e to O_2, slightly larger than that by Au_{16}^- (0.28e), Au_{17}^- (0.31e), Au_{18a}^-(0.38e), and Au_{18b}^- (0.34e), which may explain its relatively strong binding with O_2 compared to other gold clusters. In addition, the corner sites of the pyramidal Au_{20}^- possess not only a low coordination number but also a relatively small cone angle θ, which render Au_{20}^- a unique cluster for CO and O_2 adsorption. The CO adsorption energy amounts to −1.0 eV, and O_2 adsorption energy amounts to −0.66 eV.

Au_{27}−Au_{30} (Core−shell Clusters with a Single-Atom Core). The gold clusters in the size range of $N = 21-26$ undergo a series of major structural transformations from pyramidal, to tubular-like, and to core−shell structures.[39,57,58] Hence, in this size range, isomers with very different structures can be nearly degenerate in energy and thus can coexist with each other in the cluster beam of photoelectron spectroscopy (PES) experiments. Beyond $N = 26$, the core−shell structures become the dominant structural form, as demonstrated from a previous PES experiment[56] and theoretical studies.[56−58] In particular, Au_{27}^-, Au_{28}^-, and Au_{30}^- have a common feature that the core is a single Au atom, a prevailing structural feature for low-energy isomers in this size range.

Figure 2 illustrates the computed CO and O_2 adsorption energies associated with various surface sites of Au_{27}, Au_{28}, and Au_{30}. Similar to Au_{16}−Au_{18}, CO binds stronger with neutral clusters than their anionic counterparts, while O_2 binds stronger with anionic clusters than the neutral counterparts. Furthermore, as the size of clusters increases, no notable change in the CO adsorption energies is found. On the other hand, O_2 cannot bind with neutral gold clusters in this size range and bind very weakly with the anionic gold clusters.

Specifically, for Au_{27}, the strong CO binding sites are located at the two ends of the tubular-like shell while the weak binding sites are located in the middle region, especially for the anionic Au_{27}^- (Figure 2). The CO adsorption energy amounts to −1.03 eV for the anion and −1.09 eV for the neutral. Likewise, the relatively strong O_2 binding sites are located at the two ends of the tubular-like shell. Calculated adsorption energy of O_2 amounts to −0.28 eV for the anion and −0.14 eV for the neutral. In the middle region, however, some surface sites with the coordination number six are favorable binding sites while others are unfavorable binding sites for either CO or O_2. Further examination shows

that the six-coordinated sites with relatively small cone angles (80−100°) are the favorable binding sites, while others with relatively large cone angles (110−160°) are unfavorable binding sites. We conclude that the cone angle θ of a surface site is an alternative important factor for the CO and O_2 adsorption strength in addition to the low coordination number.

Au_{28} possesses several four- and five-coordinated vertices which are considerably more favorable for the CO and O_2 adsorption than the six-coordinated sites on the surface. Obviously, the four- and five-coordinated vertices all entail relatively smaller cone angles than the six-coordinated vertices, consistent with our previous conclusion that the smaller cone angle plays an important role for enhancing the CO and O_2 adsorption. Au_{30} possesses a few more strong CO binding sites than Au_{27} and Au_{28} (Figure 2). Especially, CO adsorption energy for the neutral Au_{30} amounts to −1.28 eV, much higher in magnitude than that on Au_{27} and Au_{28}. Also, for O_2 adsorption, there is a corner site with O_2 adsorption energy amounting to −0.30 eV. Again, consistent with the previous conclusion, these stronger CO or O_2 binding sites on Au_{30} all entail relatively smaller cone angle, ranging from 60 to 120°.

Au_{32}−Au_{35} (Core−Shell Clusters with 3−4 Atom Core). All Au_{32}−Au_{35} possess the core−shell structure with either three or four atoms in the core.[56] As illustrated in Figure 3, the neutral species bind CO slightly stronger than the anionic counterparts, while they bind O_2 slightly weaker than their anionic counterparts. Overall, CO adsorption energies for anionic and neutral Au_{32}, Au_{33}, and Au_{35} are more or less the same but notably lower than smaller gold clusters. However, Au_{34} is an exception as it binds with CO and O_2 much more strongly than many other gold clusters.

For Au_{32}, most three- to five-coordinated sites are relatively strong CO binding sites. These sites may be viewed as corner sites with notably smaller cone angle θ compared to other surface sites or edge sites. For both anionic and neutral Au_{32}, CO adsorption energies range from −0.41 to −0.96 eV, whose magnitudes are less than those for Au_{28}−Au_{30}. Note that the neutral Au_{32} cannot adsorb O_2 due to the endothermic adsorption of O_2 on all surface sites. The anionic Au_{32}^- possesses only a single O_2 binding site with adsorption energy of −0.30 eV. Note also that an icosahedral hollow cage structure has been predicted to be the global minimum of neutral Au_{32}.[59] Site-dependent adsorption energy scheme of this isomer is shown in Supporting Information Figure S1. The CO adsorption energy is −0.88 eV on five-coordinated sites and −0.44 eV on six-coordinated sites. However, none of these sites favors O_2 adsorption.

Au_{33} is a core−shell cluster with a smoother surface compared to Au_{32} (Figure 3), hence it has less corner sites. Like other clusters, the surface sites with larger cone angles (θ > 150°) are relatively weak CO and O_2 binding sites, while those with smaller cone angles (θ < 130°) are relatively strong binding sites. The magnitude of CO adsorption energies for anionic and neutral Au_{33} is less than that for Au_{32}, but the magnitude of O_2 adsorption energy is greater than that for Au_{32}^-.

Like Au_{20}, Au_{34} is an electronic magic-number cluster (due to shell-closing) with a relatively large HOMO−LUMO gap compared to neighboring gold clusters.[53,56] Remarkably, DFT calculations show that this cluster is also very special due to its relatively strong CO and O_2 adsorption capability than neighboring gold clusters. About a half total number of surface sites of Au_{34} are very favorable for the CO adsorption with adsorption energies amounting to −0.9 eV. Moreover, neutral Au_{34} has a single favorable O_2 binding site with exothermic adsorption energy of −0.32 eV. However, for Au_{34}^-, there exist four endothermic O_2 binding sites, indicating that a majority of surface sites of Au_{34}^- are favorable to adsorb O_2 compared to smaller clusters Au_{27}^-, Au_{28}^-, Au_{30}^-, Au_{32}^-, and Au_{33}^-. This relatively strong O_2 adsorption capability on a majority of surface sites is crucial for higher catalytic activities (see below).

Au_{35}^- has a strong CO binding site with exothermic adsorption energy of −0.96 eV and many relatively weak CO binding sites with exothermic adsorption energies ranging from −0.46 to −0.89 eV. On neutral Au_{35}, CO can bind strongly with the tip site (see Figure 3) and a few corner sites, with adsorption energy being <−0.90 eV. Like Au_{27}−Au_{33}, the neutral Au_{35} is not a good adsorbent for O_2. We also find that the tip site of Au_{35}^- is the only surface site that can adsorb O_2 with adsorption energy of −0.22 eV. Hence, this site is likely the only active site for the CO oxidation.

Catalytic Activities in Gas Phase. Previous studies have shown that coadsorption of CO and O_2 on a gold cluster is the crucial initial step for CO oxidation.[25,26,41−52] However, few systematic studies have been reported on the site-size-activity relationship, particularly the correlation, on a surface-site-by-surface-site base, between the CO and O_2 adsorption capabilities and activation energies. Having obtained CO and O_2 adsorption energies on every distinctive surface site for all anionic and neutral clusters considered, we have attempted to identify all active sites on the gold clusters, thereby gaining deeper insights into the site-size-activity relationship for the CO oxidation in the gas phase. Note that we have also tested different adsorption sites for O_2, including the top, bridge, and hollow sites, while CO is located on a neighbor top site. We find that, after geometric optimization, coadsorbed CO and O_2 both end up the top configuration of neighbor sites (see Figure S2).

Clusters Size versus Catalytic Activities. The reaction mechanism for the CO oxidation on bare or doped gold clusters has been studied previously.[14−17,60−69] In Figures 4 and 5, we display catalytic reaction pathways for the CO oxidation on the strongest CO and O_2 bind

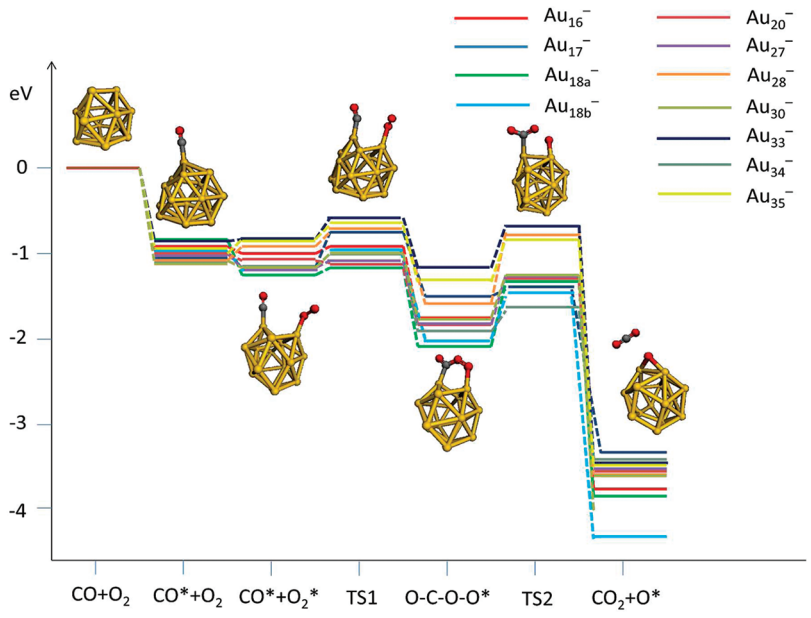

Figure 4. Computed reaction pathways of $CO + O_2 \rightarrow CO_2 + O$ associated with various anionic gold clusters in the size range of Au_{16}^{-}–Au_{35}^{-}. Here, * denotes the adsorbed species on a gold cluster. Corresponding numerical values are given in Table 1.

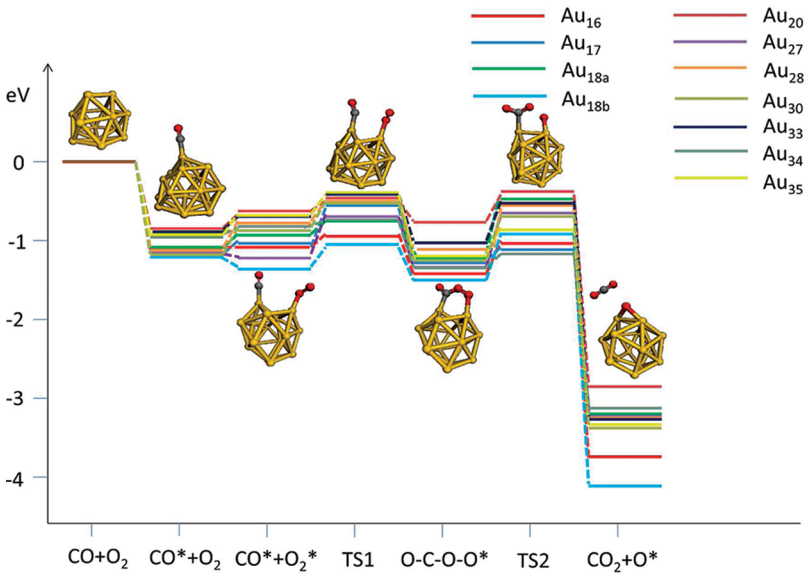

Figure 5. Reaction pathways of $CO + O_2 \rightarrow CO_2 + O$ associated with various neutral gold clusters in the size range of Au_{16} to Au_{35}. Here, * denotes the adsorbed species on a gold cluster. Corresponding numerical values are given in Table 2. The reaction pathway associated with neutral icosahedral cage isomer of Au_{32} is plotted in Figure S3.

sites of anionic and neutral gold clusters in the size range of Au_{16}–Au_{35}. As the initial step, CO and O_2 are coadsorbed on the gold clusters (known as the Langmuir–Hinshelwood mechanism). Consistent with our recent theoretical results for gold nanotube and crown gold cluster,[62,63] we confirm that preadsorption of a CO molecule on gold clusters can indeed enhance O_2 adsorption, especially for the smaller gold clusters ($N \leq 20$). For example, the calculated CO and O_2 adsorption energies on Au_{16}^{-} are −0.90 and −0.02 eV, respectively, while the coadsorption energy of both CO and O_2 molecules is −1.01 eV, which differs by −0.09 eV from the sum of −0.90 and −0.02 eV. The gain in adsorption energy could be attributed to the effect of charge transfer; for example, for Au_{16}^{-}, CO preadsorbed gold cluster donates 0.30e to O_2, larger than the charge donated by bare Au_{16}^{-} (0.26e). Moreover, although the CO adsorption is more favorable on neutral clusters than on anionic clusters, the coadsorption of CO and O_2 on anionic clusters is stronger than that on neutral counterparts. Our results suggest that the catalytic reaction is more favorable on anionic clusters than on neutral counterparts. We also note that the effect of coadsorption becomes weaker with

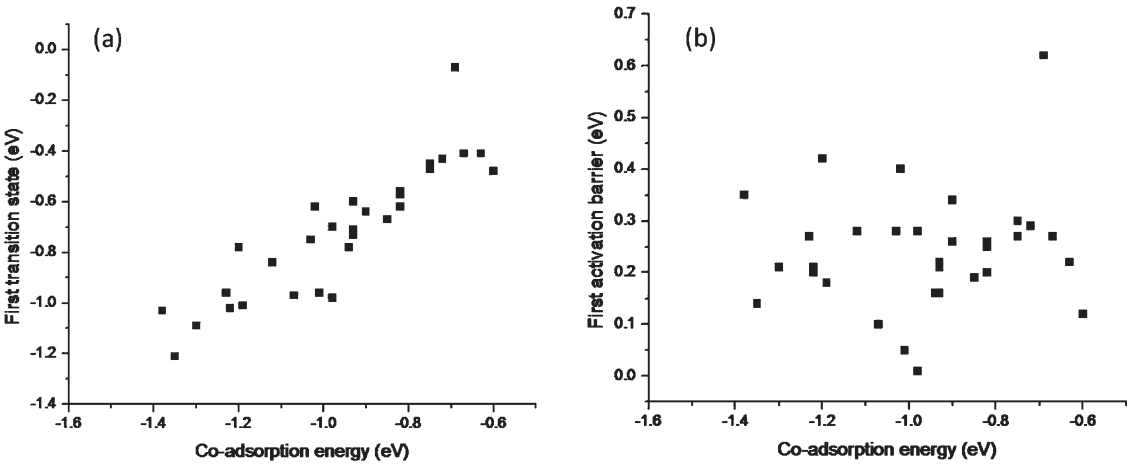

Figure 6. (a) Coadsorption energy (eV) *versus* energy level of the first transition state (eV). (b) Coadsorption energy (eV) *versus* the first activation barrier (eV).

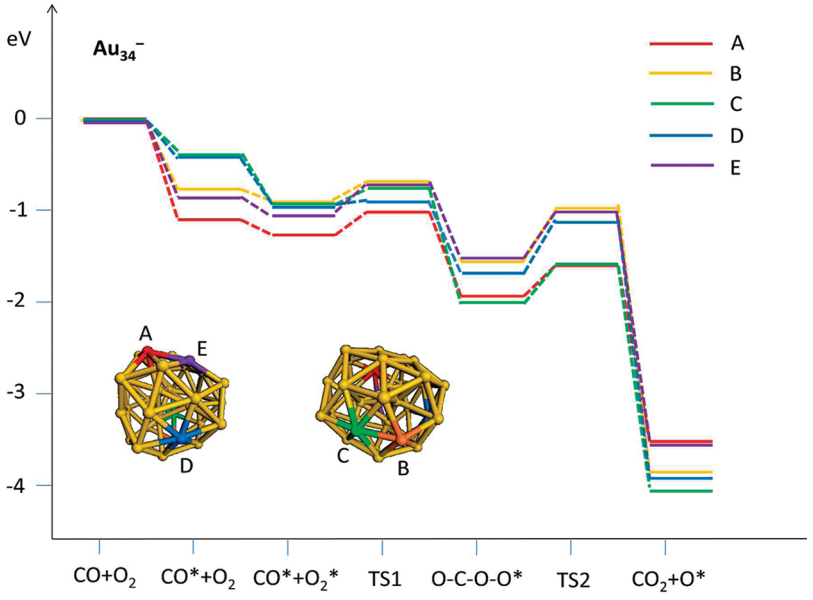

Figure 7. Calculated reaction pathways corresponding to five surface sites (A–E) on Au_{34}^-. The five sites are highlighted on the cluster (inset).

increasing the size of gold clusters, suggesting that the smaller gold clusters generally entail higher catalytic capabilities, although exception may occur with magic-number clusters (see below).

In the second step, CO and O_2 move closer to each other, followed by crossing of the first energy barrier (TS1 shown in Figures 4 and 5) to form the intermediate complex O–C–O–O* with a C–O single bond (bond length ~1.37 Å) and a peroxide O–O bond (bond length ~1.44 Å). Comparing Figures 4 with 5, one can see that the reaction barriers associated with anionic clusters are indeed lower than those associated with the neutral counterparts. In particular, both anionic and neutral Au_{16} and Au_{20} give rise to very low reaction barriers. For Au_{20}^-, the first step is actually barrier-less, and for Au_{16}^-, the computed reaction barrier is merely 0.05 eV. For neutral Au_{16} and Au_{20}, the barriers are also very low (0.10 and 0.12 eV, respectively). The reaction barriers for larger anionic clusters range from 0.14 to 0.27 eV. Au_{17}^- is an exception, which exhibits a relatively high reaction barrier of 0.42 eV. The reaction barriers for other neutral clusters range from 0.20 to 0.40 eV. It appears that beyond Au_{20} the reaction barriers for the second step do not change much, suggesting that the size of subnanometer gold clusters is not a crucial parameter to affect the second reaction barrier. Note also by comparing Figures 4 with 5 that the intermediate complexes associated with anionic clusters appear to be lower in energy than those associated with the neutral counterparts. This result supports again that the CO oxidation is more favorable on the anionic gold clusters than on the neutral counterparts.

Subsequent to formation of the intermediate complex O–C–O–O*, the labile peroxide O–O bond will

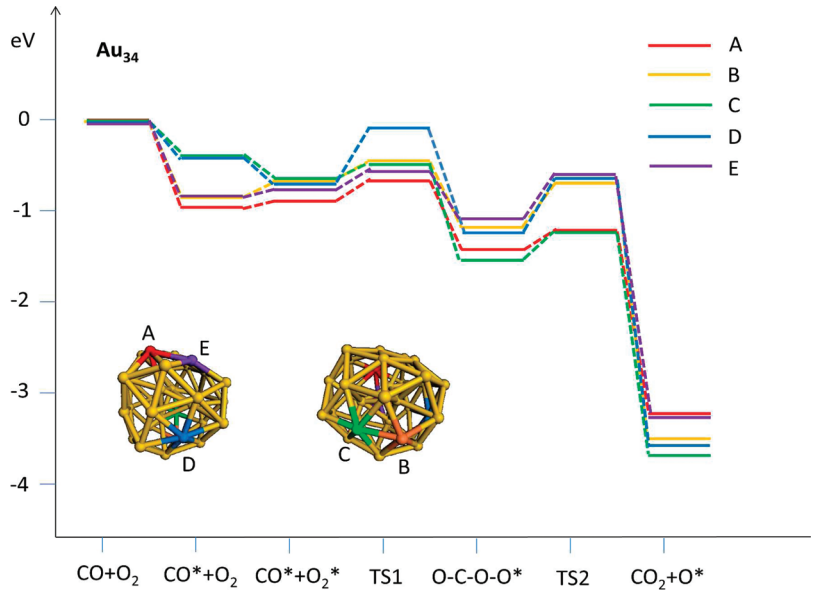

Figure 8. Calculated reaction pathways corresponding to five surface sites (A−E) on Au_{34}. The five sites are highlighted on the cluster (inset).

TABLE 1. Computed Relative Energies (eV), with Respect to the Reactant in the Gas Phase, of Initial CO Adsorption States, Coadsorption States, First Transition States (TS1), Intermediate States (IS), Second Transition States (TS2), and the Final States for the CO Oxidation on Various Anionic Gold Clusters in the Size Range of Au_{16}^-−Au_{35}^-

	CO adsorption	[CO + O_2] adsorption	IS		TS2	CO_2 + O adsorption
			TS1	(O−C−O−O*)		
Au_{16}^-	−0.90	−1.01	−0.96	−1.72	−1.25	−3.72
Au_{17}^-	−1.03	−1.20	−0.78	−1.54	−1.38	−3.38
Au_{18a}^-	−0.89	−1.35	−1.21	−2.05	−1.34	−3.84
Au_{18b}^-	−0.98	−1.23	−0.96	−2.01	−1.41	−4.36
Au_{20}^-	−1.00	−1.09		−1.78	−1.34	−3.66
Au_{27}^-	−1.02	−1.30	−1.09	−1.77	−1.22	−3.60
Au_{28}^-	−1.05	−0.93	−0.71	−1.48	−0.79	−3.63
Au_{30}^-	−1.18	−1.19	−1.01	−1.71	−1.33	−4.01
Au_{32}^-	−0.91	−0.93	−0.77	−1.43	−0.90	−3.44
Au_{33}^-	−0.88	−0.85	−0.60	−1.17	−0.69	−3.57
Au_{34}^-	−1.05	−1.22	−1.02	−1.92	−1.68	−3.48
Au_{35}^-	−0.95	−0.86	−0.67	−1.36	−0.86	−3.69

TABLE 2. Computed Relative Energies (eV), with Respect to the Reactant in the Gas Phase, of Initial Coadsorption States, First Transition States (TS1), Intermediate States (IS), Second Transition States (TS2), and the Final States for the CO Oxidation on Various Neutral Gold Clusters in the Size Range of Au_{16}−Au_{35}

	CO adsorption	[CO + O_2] adsorption	IS		TS2	CO_2 + O adsorption
			TS1	(O−C−O−O*)		
Au_{16}	−1.08	−1.07	−0.97	−1.46	−1.03	−3.80
Au_{17}	−1.13	−1.02	−0.62	−1.28	−1.09	−3.23
Au_{18}-iso1	−1.07	−0.98	−0.70	−1.29	−0.57	−3.22
Au_{18}-iso2	−1.16	−1.38	−1.03	−1.52	−0.96	−4.10
Au_{20}	−0.87	−0.60	−0.48	−0.88	−0.45	−2.90
Au_{27}	−1.09	−1.12	−0.84	−1.38	−0.80	−3.29
Au_{28}	−1.05	−0.82	−0.56	−1.09	−0.69	−3.39
Au_{30}	−1.19	−0.82	−0.57	−1.34	−0.66	−3.42
Au_{32}	−0.95	−0.82	−0.62	−1.16	−0.67	−3.68
Au_{33}	−0.95	−0.75	−0.45	−1.03	−0.60	−3.36
Au_{34}	−0.98	−0.90	−0.64	−1.39	−1.16	−3.16
Au_{35}	−0.96	−0.72	−0.43	−1.21	−0.94	−3.46

dissociate *via* crossing the second energy barrier (TS2 in Figures 4 and 5), resulting in a free CO_2 molecule and an atomic O on the cluster surface. Our calculation indicates that the second reaction barrier ranges from 0.16 eV (Au_{17}^-) to 0.71 eV (Au_{18a}^-) for anionic clusters and from 0.19 eV (Au_{17}) to 0.72 eV (Au_{18a}) for neutral clusters. These reaction barriers are comparable to those associated with smaller-sized gold clusters (~0.40 eV)[24−26,41−52] but higher than those on endohedral doped gold clusters (0.05−0.27 eV for W@Au_{12} and Na@Au_{17}).[45,49] Remarkably, the second reaction barriers associated with the magic-number cluster Au_{34} (Au_{34}^-, 0.24 eV; Au_{34}, 0.23 eV) are notably lower than those of neighboring clusters (0.38−0.69 eV for anionic and 0.27−0.68 eV for neutral clusters).

Finally, to complete the catalytic cycle, the adsorbed atomic oxygen should be removed. In fact, the atomic O can interact with the CO molecule directly to form second CO_2 (Eley−Rideal mechanism). The calculated activation energy barriers of this final step are given in Table 3. The reactions, in general, entail low activation barrier reactions (some are even barrierless), consistent with previous conclusions that this last step is not a rate-limiting step,[43−45,63] and the reactions on anionic clusters have lower barriers than those on neutral clusters.

In Figure 6a,b, we plot coadsorption energies of CO and O_2 *versus* energy levels of the first transition state and the activation barrier of TS1, respectively. It appears that coadsorption energies do not correlate with

TABLE 3. Calculated Activation Energy Barriers (eV) and Geometric Parameters at the Transition State for CO + O* → CO_2 on Anionic and Neutral Au Clusters[a]

	anion			neutral		
	ΔE_a (eV)	Au−O* (Å)	C−O* (Å)	ΔE_a (eV)	Au−O* (Å)	C−O* (Å)
Au_{16}	0.15	2.483	1.866	0.30	2.393	1.809
Au_{17}				0.01	2.088	1.877
Au_{18a}	0.05	2.436	1.957	0.11	2.251	2.044
Au_{18b}	0.07	2.210	1.787	0.58	2.338	1.865
Au_{20}						
Au_{27}				0.14	2.284	1.922
Au_{28}	0.31	2.403	1.886	0.23	2.223	1.952
Au_{30}				0.08	2.168	1.964
Au_{32}				0.28	2.413	1.484
Au_{33}	0.04	2.288	1.824	0.11	2.240	1.856
Au_{34}	0.33	2.164	1.895	0.32	2.169	2.052
Au_{35}	0.16	2.223	1.839	0.31	2.192	1.949

[a] O* represents the O atom adsorbed on the surface of Au clusters. Empty line denotes no barrier for the reaction.

the activation barriers, but the energy levels of the first transition state show some correlation. However, it is the activation barrier associated with the first transition state that determines the catalytic efficiency, as shown in the kinetic analysis in the Supporting Information.

Site-Specific Adsorption Energies versus Catalytic Activities for Magic-Number Cluster Au_{34}. Correlation between the site-specific adsorption energy and the cluster's catalytic activity has not been systematically explored for medium-sized gold clusters. Here, we select five distinctive surface sites (with different CO and O_2 adsorption energies) on a magic-number cluster Au_{34} to investigate whether there is a strong correlation between adsorption energy and catalytic activity. Computed reaction pathways for the CO oxidation on the anionic Au_{34}^- and neutral Au_{34} are shown in Figures 7 and 8, respectively. In Figure 7, one can see that the weaker CO binding site can adsorb O_2 more strongly. As an example, site A is a relatively strong CO binding site (with adsorption energy −1.05 eV), while its neighbor site yields the O_2 adsorption energy of −0.20 eV. The coadsorption energy of CO and O_2 molecules on the same two sites is −1.22 eV, very close to the sum of −1.05 and −0.20 eV. In contrast, site C is a relatively weak CO binding site (with adsorption energy −0.42 eV), while its neighbor site yields O_2 adsorption energy of −0.03 eV. The coadsorption energy of CO and O_2 on the same two sites is −0.94 eV, much greater in magnitude than the sum of −0.42 and −0.03 eV. However, this larger difference between the coadsorption energy and the sum of individual adsorption energies for the weak CO binding site cannot fully offset the difference in CO adsorption energies between the weak and strong CO binding sites. Hence, the coadsorption state associated with the site A still entails a lower energy level than those associated with other four sites (B−E). On the other hand, the coadsorption of CO and O_2 is much more weakly on the neutral Au_{34} than the anionic Au_{34}^- due to stronger endothermic O_2 adsorption on Au_{34}. More specifically, computed coadsorption energies on site A of Au_{34}^- and Au_{34} are −1.22 and −0.90 eV, respectively, while those on site C are −0.94 and −0.63 eV, respectively (see Tables 1 and 2).

The second step involves the formation of the intermediate O−C−O−O* complex *via* crossing the first reaction barrier. On Au_{34}^-, both site A and site E are relatively strong sites for coadsorption of CO and O_2 molecules (site A, −1.22 eV; site E, −1.04 eV), and the corresponding reaction barrier at the TS1 state (see Figure 7) is 0.21 and 0.27 eV, respectively. As a comparison, site C and site D on Au_{34}^- are relatively weaker site for coadsorption of CO and O_2 (site C, −0.93 eV; site D, −0.98 eV), and both sites yield a lower reaction barrier at the TS1 state (0.16 and 0.01 eV, respectively). However, since the energy level of the transition state (TS1) associated with the site A is still the lowest among the five sites considered, the site A, with the strongest coadsorption with CO and O_2, is likely the most active site in this oxidation step (see Supporting Information for a simple kinetics analysis), even though the energy level of the intermediate state associated with site C (the weakest CO bind site) is lower than that associated with site A (the strongest CO binding site) on Au_{34}^- and Au_{34}. This result suggests that the adsorption strength can play an important role in the oxidation rate, even though they are not correlated with the stability of the intermediate complex.

In the second barrier-crossing step, the intermediate O−C−O−O* complex forms a free CO_2 molecule and an atomic O. Among the five surface sites considered, site A gives rise to the lowest reaction barrier (Au_{34}^-, 0.24 eV; Au_{34}, 0.23 eV) and site C gives the second lowest barrier (Au_{34}^-, 0.34 eV; Au_{34}, 0.32 eV) in the final step. The other three sites give relatively higher but similar reaction barriers (Au_{34}^-, ∼0.55 eV; Au_{34}, ∼0.50 eV). These results suggest that reactant adsorption strengths are not directly correlated with the second reaction barrier. Hence, the limiting step of the reaction is likely attributed to preadsorption of CO in the oxidation step, consistent with the previous theoretical studies.[70]

CONCLUSIONS

The CO oxidation on subnanometer anionic gold clusters and their neutral counterparts has been systematically studied by using *ab initio* calculations. Several conclusions drawn from these calculations include the following: (1) Compared to the neutral clusters, the extra negative charge on the anionic clusters can enhance not only O_2 adsorption but also the strength of coadsorption of CO and O_2, which leads to a lower reaction barrier in the oxidation step. Recent

experimental studies revealed that negatively charged gold clusters on TiO_2[71−73] and MgO[24] surfaces can enhance catalytic activity, which support our theoretical results. (2) The strength of coadsorption of CO and O_2 molecules becomes weaker as the size of gold clusters increases, except the magic-number cluster Au_{34}, which possesses exceptional binding capability with CO and O_2 compared to its neighboring clusters. (3) In addition to the low coordination number, relatively small cone angle (<110°) associated with each surface site is another important geometric indicator of relatively strong adsorption strength of CO or O_2 (see Figure S4 in the Supporting Information). (4) Computation of reaction pathways on various distinctive sites of gold clusters with the *core*−*shell* structure indicates that the reaction barriers are not very sensitive to the size of clusters (except the magic-number cluster Au_{34}). However, for hollow cage and pyramidal gold clusters, the reaction barriers can be very sensitive to the size of clusters. (5) For the magic-number cluster Au_{34}, our calculations show that preadsorption of CO can further enhance adsorption strength of O_2, but only at relatively weak CO binding sites (not at relatively strong CO binding sites). In addition, we find no apparent correlation between the local adsorption strength of O_2 and the Hirshfeld charge at the same atomic site (see Figures S5 and S6). (6) Lastly, strong coadsorption of CO and O_2 lowers the barrier corresponding to the first transition state (in the oxidation step) but has little effect on the stability of the intermediate and the barrier of the second transition state. These conclusions provide additional insights into the site-size-activity relationships for the subnanometer gold clusters. Also, our calculation supports the notion that relatively strong adsorption of reactants on a catalyst is a key factor for the efficiency of the CO oxidation.

COMPUTATIONAL METHODS

Geometric structures of all of the gold clusters considered in this study, with adsorbed CO and/or O_2, are optimized using an unrestricted density functional theory (DFT) method within the general gradient approximation in the form of Perdew−Burke−Ernzerhof (PBE) functional.[74] Semicore pseudopotential is opted together with the double numerical plus polarization (DNP) basis set for the geometric optimization.[75,76] The adsorption energies of CO and O_2 on the gold clusters are calculated according to the formula $\Delta E_{ad} = E(\text{Au-CO/O}_2) - E(\text{Au}) - E(\text{CO/O}_2)$. The reaction pathways for the CO oxidation are computed using the combination of LST/QST algorithm with subsequent conjugated gradient method, and all transition states are further confirmed by the nudged elastic band (NEB) method.[77,78] All computations are performed using the DMol^3 4.3 software package.[75,76]

In the calculation of reaction pathways, the spin states of a free-standing O_2 and O_2 preadsorbed Au clusters with totally even number of valence electrons are set as triplet, while O_2 preadsorbed Au clusters with totally odd number of valence electrons are set as doublet. In all subsequent states, including all transition states, intermediate states, and final states, the spin states of the system are set as the lowest spin states. During geometrical optimization, the energy convergence is 2.0×10^{-5} Hartree, the gradient convergence is 4.0×10^{-3} Å, and the displacement convergence is 5.0×10^{-3} Å. In the NEB transition state search process, the threshold for SCF convergence is 10^{-5} Hartree, charge mixing is 0.1, spin mixing is 0.2, and rms convergence is 0.01. The smearing is set as 0.005 Hartree to accelerate the convergence. The triplet−singlet crossover is not considered when searching for the transition states, but the relative stabilities between triplet and singlet spin states of the transition states are examined.

Once the transition state structure is attained through NEB search, vibrational frequency analysis is performed to ensure that the transition state has only one significant imaginary vibrational frequency. Minor imaginary vibrational frequencies whose magnitude is less than 40 cm^{-1} are ignored. In Tables S1 and S2, geometries of the computed transition states and intermediate states are presented for the purpose of cross examination. We note that these geometries are very close to those previously reported with either gold cluster or gold surface systems,[43,44,49,79,80] which provides independent confirmation on the computed reaction pathways presented in this paper.

Acknowledgment. This work is supported by grants from NSF (EPS-1010674, EPS-1010094), ARL (W911NF1020099), and a seed grant by the Nebraska Center for Energy Sciences Research, and by the University of Nebraska Holland's Computing Center. Y.P. is partially supported by the Academic Leader Program in Xiangtan University (10QDZ34) and Natural Science Foundation of China (Grant No. 21103144).

Supporting Information Available: Adsorption energies and reaction pathways associated with the icosahedral hollow cage neutral isomer of Au_{32}, adsorption energies *versus* cone angles for anion clusters considered, a test calculation for the most stable adsorption configuration for O_2, and a simple kinetic analysis for Au_{34} are collected. This material is available free of charge *via* the Internet at http://pubs.acs.org.

REFERENCES AND NOTES

1. Haruta, M.; Kobayashi, T.; Samo, H.; Yamada, N. Novel Gold Catalysts for the Oxidation of Carbon Monoxide at a Temperature Far Below 0 °C. *Chem. Lett.* **1987**, 405–408.
2. Haruta, M.; Yamada, N.; Kobayashi, T.; Ijima, S. Gold Catalysts Prepared by Coprecipitation for Low-Temperature Oxidation of Hydrogen and of Carbon Monoxide. *Catal. Today* **1989**, *115*, 301–308.
3. Lizuka, Y.; Fujiki, H.; Yamauchi, N.; Chijiiwa, T.; Arai, S.; Tsubota, S.; Haruta, M. Adsorption of CO on Gold Supported on TiO_2. *Catal. Today* **1997**, *36*, 115–123.
4. Haruta, M. Size and Support-Dependency in the Catalysis of Gold. *Catal. Today* **1997**, *36*, 153–166.
5. Bond, G. C. Gold: A Relatively New Catalyst. *Catal. Today* **2002**, *72*, 5–9.
6. Grabow, L. C.; Mavrikakis, M. Nanocatalysis beyond the Gold-Rush Era. *Angew. Chem., Int. Ed.* **2008**, *47*, 7390–7392.
7. Hutchings, G. J.; Burst, M.; Schmidbaur, H. Gold—An Introductory Perspective. *Chem. Soc. Rev.* **2008**, *37*, 1759–1765.
8. Daniel, M.-C.; Astruc, D. Gold Nanoparticles: Assembly, Supremolecular Chemistry, Quantum-Size Related Properties, and Applications toward Biology, Catalysis and Nanotechnology. *Chem. Rev.* **2004**, *104*, 293–346.
9. Pyykkö, P. Theoretical Chemistry of Gold. *Angew. Chem., Int. Ed.* **2004**, *43*, 4412–4456.
10. Pyykkö, P. Theoretical Chemistry of Gold. III. *Chem. Soc. Rev.* **2008**, *37*, 1967–1997.

11. Pina, C. D.; Falletta, E.; Prati, L.; Rossi, M. Selective Oxidation Using Gold. *Chem. Soc. Rev.* **2008**, *37*, 2077–2095.
12. Pyykkö, P. *Relativistic Theory of Atoms and Molecules*; Springer: Berlin, 2000; Vol. III, pp 108−111.
13. Schwarz, H. Relative Effects in Gas-Phase Ion Chemistry: An Experimentalist's View. *Angew. Chem., Int. Ed.* **2003**, *42*, 4442–4454.
14. Wesendrup, R.; Hunt, T.; Schwerdtfeger, P. Relativistic Coupled Cluster Calculations for Neutral and Singly Charged Au_3 Clusters. *J. Chem. Phys.* **2000**, *112*, 9356–9362.
15. Häkkinen, H.; Landman, U. Gold Clusters (Au_N, $2 < N < 10$) and Their Anions. *Phys. Rev. B* **2000**, *62*, R2287–R2290.
16. Häkkinen, H.; Moseler, M.; Landman, U. Bonding in Cu, Ag and Au Clusters: Relativistic Effects, Trends and Surprises. *Phys. Rev. Lett.* **2002**, *89*, 033401.
17. Hashmi, A. S. K.; Hutchings, G. J. Gold Catalysis. *Angew. Chem., Int. Ed.* **2006**, *45*, 7896–7936.
18. Chen, M. S.; Goodman, D. W. Catalytically Active Gold: From Nano-particles to Ultra-thin Film. *Acc. Chem. Res.* **2006**, *39*, 739–746.
19. Chen, M. S.; Goodman, D. W. Active Structure of Supported Au Catalysts. *Catal. Today* **2006**, *111*, 22–33.
20. Chen., M. S.; Goodman, D. W. Catalytically Active Gold on Ordered Titania Supports. *Chem. Soc. Rev.* **2008**, *37*, 1860–1870.
21. Bond, G. C.; Louis, C.; Thompson, D. T. *Catalysis by Gold*; Imperial College Press: London, 2006.
22. Herzing, A. A.; Kiely, C. J.; Carley, A. F.; Landon, P.; Hutchings, G. J. Identification of Active Gold Nanoclusters on Iron Oxide Supports for CO Oxidation. *Science* **2008**, *321*, 1331–1335.
23. Chen, M. S.; Goodman, D. W. The Structure of Catalytically Active Gold on Titania. *Science* **2004**, *306*, 252–255.
24. Sanchez, A.; Abbet, S.; Heiz, U.; Schneider, W.-D.; Häkkinen, H.; Barnett, R. W.; Landman, U. When Gold is Not Noble: Nanoscale Gold Catalysts. *J. Phys. Chem. A* **1999**, *103*, 9573–9578.
25. Yoon, B.; Häkkinen, H.; Landman, U.; Wörz, A. S.; Antonietti, J. M.; Abbet, S.; Judai, K.; Heiz, U. Charging Effects on Bonding and Catalyzed Oxidation of CO on Au_8 Clusters on MgO. *Science* **2005**, *307*, 403–405.
26. Lopez, N.; Nørskov, J. K. Catalytic CO Oxidation by a Gold Nanoparticle: A Density Functional Study. *J. Am. Chem. Soc.* **2002**, *124*, 11262–11263.
27. Shibata, N.; Goto, A.; Matsunaga, K.; Mizoguchi, T.; Findlay, S. D.; Yamamoto, T.; Ikuhara, Y. Interface Structures of Gold Nanoparticles on TiO_2(110). *Phys. Rev. Lett.* **2009**, *102*, 136105.
28. Zhang, C.; Michaelides, A.; King, D. A.; Jenkins, S. J. Positive Charge States and Possible Polymorphism of Gold Nanoclusters on Reduced Ceria. *J. Am. Chem. Soc.* **2010**, *132*, 2175–2182.
29. Furche, F.; Ahlrichs, R.; Weis, P.; Jacob, C.; Gilb, S; Bierweller, T.; Kappes, M. M. The Structures of Small Gold Cluster Anions as Determined by a Combination of Ion Mobility Measurements and Density Functional Calculations. *J. Chem. Phys.* **2002**, *117*, 6982–6990.
30. Xing, X; Yoon, B; Landman, U; Parks, J. H. Structural Evolution of Au Nanoclusters: From Planar to Cage to Tubular Motifs. *Phys. Rev. B* **2006**, *74*, 165423.
31. Johansson, M. P.; Lechtken, A.; Schooss, D.; Kappes, M. M.; Furche, F. 2D−3D Transition of Gold Cluster Anions Resolved. *Phys. Rev. A* **2008**, *77*, 053202.
32. Lechtken, A.; Neiss, C.; Stairs, J.; Schooss, D. Comparative Study of the Structures of Copper, Silver, and Gold Icosamers: Influence of Metal Type and Charge State. *J. Chem. Phys.* **2008**, *129*, 154304.
33. Gruene, P.; Rayner, D. M.; Redlich, B.; van der Meer, A. F. G.; Lyon, J. T.; Meijer, G.; Fielicke, A. Structures of Neutral Au_7, Au_{19}, and Au_{20} Clusters in the Gas Phase. *Science* **2008**, *321*, 674–676.
34. Lechtken, A.; Neiss, C.; Kappes, M. M.; Schooss, D. Structure Determination of Gold Clusters by Trapped Ion Electron Diffraction: Au_{14}^-−Au_{19}^-. *Phys. Chem. Chem. Phys.* **2009**, *11*, 4344–4350.
35. Häkkinen, H.; Yoon, B.; Landman, U.; Li, X.; Zhai, H. J.; Wang, L. S. On the Electronic and Atomic Structures of Small Au_N- (N = 4−14) Clusters: A Photoelectron Spectroscopy and Density-Functional Study. *J. Phys. Chem. A* **2003**, *107*, 6168–6175.
36. Yoon, B.; Koskinen, P.; Huber, B.; Kostko, B.; Issendorff, B. v.; Häkkinen, H; Moseler, M.; Landman, U. Size-Dependent Structural Evolution and Chemical Reactivity of Gold Clusters. *ChemPhysChem* **2007**, *8*, 157–161.
37. Li, J.; Li, X.; Zhai, H. J.; Wang, L. S. Au_{20}: A Tetrahedral Cluster. *Science* **2003**, *299*, 864–867.
38. Bulusu, S.; Li, X.; Wang, L. S.; Zeng, X. C. Evidence of Hollow Gold Cages. *Proc. Natl. Acad. Sci. U.S.A.* **2006**, *103*, 8326–8330.
39. Bulusu, S.; Li, X.; Wang, L. S.; Zeng, X. C. Structural Transitions from Pyramidal to Fused Planar to Tubular to Core/Shell Compact in Gold Clusters: Au_n^- (n = 21−25). *J. Phys. Chem. C* **2007**, *111*, 4190–4198.
40. Huang, W.; Bulusu, S.; Pal, R.; Zeng, X. C.; Wang, L. S. Structural Transition of Gold Nanoclusters: From the Golden Cage to the Golden Pyramid. *ACS Nano* **2009**, *3*, 1225–1230.
41. Janssens, T. V. W.; Clausen, B. S.; Hvolbaek, B.; Falsig, H.; Christensen, C. H.; Bligaard, T.; Nørskov, J. K. Insights into the Reactivity of Supported Au Nanoparticles: Combining Theory and Experiments. *Top. Catal.* **2007**, *44*, 15–26.
42. Remediakis, I. N.; Lopez, N.; Nørskov, J. K. CO Oxidation on Rutile-Supported Au Nanoparticles. *Angew. Chem., Int. Ed.* **2005**, *44*, 1824–1826.
43. Molina, L. M.; Hammer, B. Some Recent Theoretical Advances in the Understanding of the Catalytic Activity of Au. *Appl. Catal., A* **2005**, *291*, 21–31.
44. Molina, L. M.; Rasnussen, M. D.; Hammer, B. Adsorption of O_2 and Oxidation of CO at Au Nanoparticles Supported by TiO_2(110). *J. Chem. Phys.* **2004**, *120*, 7673–7680.
45. Molina, L. M.; Hammer, B. The Activity of the Tetrahedral Au_{20} Cluster: Charging and Impurity Effects. *J. Catal.* **2005**, *233*, 399–404.
46. Socaciu, L. D.; Hagen, J.; Bernhardt, T. M.; Woste, L.; Heiz, U.; Häkkinen, H.; Landman, U. Catalytic CO Oxidation by Free Au_2^-: Experiment and Theory. *J. Am. Chem. Soc.* **2003**, *125*, 10437–10455.
47. Bernhardt, T. M. Gas-Phase Kinetics and Catalytic Reactions of Small Silver and Gold Clusters. *Int. J. Mass Spectrom.* **2005**, *243*, 1–29.
48. Popolan, D. M.; Bernhardt, T. M. Communication: CO Oxidation by Silver and Gold Cluster Cations: Identification of Different Active Oxygen Species. *J. Chem. Phys.* **2011**, *134*, 091102.
49. Gao, Y.; Shao, N.; Bulusu, S.; Zeng, X. C. Effective CO Oxidation on Endohedral Nanoclusters. *J. Phys. Chem. C* **2008**, *112*, 8234–8238.
50. Li, H.; Pei, Y.; Zeng, X. C. Two-Dimensional to Three-Dimensional Structural Transition of Gold Cluster Au_{10} during Soft Landing on TiO_2 Surface and Its Effect on CO Oxidation. *J. Chem. Phys.* **2010**, *133*, 134707.
51. Davran-Candan, T.; Gunay, M. E.; Yildirim, R. Structure and Activity Relationship for CO and O_2 Adsorption over Gold Nanoparticles Using Density Functional Theory and Artificial Neural Networks. *J. Chem. Phys.* **2010**, *132*, 174113.
52. Kuang, X. J.; Wang, X. Q.; Liu, G. B. All-Electron Scalar Relativistic Calculation on the Adsorption of Carbon Monoxide onto Small Gold Clusters. *Catal. Lett.* **2010**, *137*, 247–254.
53. Lechtken, A.; Schooss, D.; Stairs, J. R.; Blom, M. N.; Furche, F.; Morgner, N.; Kostko, O.; von Issendorff, B.; Kappes, M. M. Au_{34}^-: A Chiral Gold Cluster? *Angew Chem., Int. Ed.* **2007**, *46*, 2944–2947.
54. Gu, X.; Bulusu, S.; Li, X.; Zeng, X. C.; Li, J.; Gong, X. G.; Wang, L. S. Au_{34}^-: A Fluxional Core−Shell Cluster. *J. Phys. Chem. C* **2007**, *111*, 8228–8232.
55. Huang, W.; Ji, M.; Dong, C. D.; Gu, X.; Wang, L. M.; Gong, X. G.; Wang, L. S. Relativistic Effects and the Unique Low-

Symmetry Structures of Gold Nanoclusters. *ACS Nano* **2008**, *2*, 897–904.
56. Shao, N.; Huang, W.; Gao, Y.; Wang, L. M.; Li, X.; Wang, L. S.; Zeng, X. C. Probing the Structural Evolution of Medium-Sized Gold Clusters: Au_n^- (n = 27−35). *J. Am. Chem. Soc.* **2010**, *132*, 6596–6605.
57. Luo, C. F.; Fa, W.; Dong, J. M. Adsorption of O_2 on Tubelike Au_{24} and Au_{24}^- Clusters. *J. Chem. Phys.* **2006**, *125*, 084707.
58. Tian, D.; Zhao, J. Competition Among fcc-Like, Double-Layered Flat, Tubular Cage, and Close-Packed Structural Motifs for Medium-Sized Au_n (n = 21−28) Cluster. *J. Phys. Chem. A* **2008**, *112*, 3141–3144.
59. Johansson, M. P.; Sundholm, D.; Vaara, J. Au_{32}: A 24-Carat Golden Fullerene. *Angew. Chem., Int. Ed.* **2004**, *43*, 2678–2681.
60. De Bocarme, T. V.; Chau, T. D.; Tielens, F.; Andres, J.; Gaspard, P.; Wang, R. L. C.; Kreuzer, H. J.; Kruse, N. Oxygen Adsorption on Gold Nanofacets and Model Clusters. *J. Chem. Phys.* **2006**, *125*, 054703.
61. McKenna, K. P.; Shluger, A. L. Shaping the Morphology of Gold Nanoparticles by CO Adsorption. *J. Phys. Chem. C* **2007**, *111*, 18848–18852.
62. An, W.; Pei, Y.; Zeng, X. C. CO Oxidation Catalyzed by Single-Walled Helical Gold Nanotube. *Nano Lett.* **2008**, *8*, 195–202.
63. Gao, Y.; Shao, N.; Pei, Y.; Zeng, X. C. Icosahedral Crown Gold Nanocluters $Au_{43}Cu_{12}$ with High Catalytic Activity. *Nano Lett.* **2010**, *10*, 1055–1062.
64. Bernhardt, T. M.; Hagen, J.; Lang, S. M.; Popolan, D. M.; Socaciu-Siebert, L. D.; Woste, L. Binding Energies of O_2 and CO to Small Gold, Silver, and Binary Silver−Gold Cluster Anions from Temperature Dependent Reaction Kinetics Measurements. *J. Phys. Chem. A* **2009**, *113*, 2724–2733.
65. Prestianni, A.; Martorana, A.; Labat, F.; Ciofini, I.; Adamo, C. Theoretical Insights on O_2 and CO Adsorption on Neutral and Positively Charged Gold Clusters. *J. Phys. Chem. B* **2006**, *110*, 12240–12248.
66. Prestianni, A.; Martorana, A.; Labat, F.; Ciofini, I.; Adamo, C. A DFT Investigation of CO Oxidation over Neutral and Cationic Gold Clustes. *J. Mol. Struct. (THEOCHEM)* **2009**, *903*, 34–40.
67. Roldán, A.; González, S.; Ricart, J. M.; Illas, F. Critical Size for O_2 Dissociation by Au Nanoparticles. *ChemPhysChem* **2009**, *10*, 348–351.
68. Wong, K.; Zeng, Q. H.; Yu, A. B. Gold Catalysts: A New Insight into the Molecular Adsorption and CO Oxidation. *Chem. Eng. J.* **2009**, *155*, 824–828.
69. Xie, Y. P.; Gong, X. G. First-Principles Studies for CO and O_2 on Gold Nanocluster. *J. Chem. Phys.* **2010**, *132*, 244302.
70. Chang, C. M.; Cheng, C.; Wei, C. M. CO Oxidation on Unsupported Au_{55}, Ag_{55} and $Au_{25}Ag_{30}$ Nanoclusters. *J. Chem. Phys.* **2008**, *128*, 124710.
71. Jiang, Z.; Zhang, W.; Jin, L.; Yang, X.; Xu, F.; Zhu, J.; Huang, W. Direct XPS Evidence for Charge Transfer from a Reduced Rutile TiO_2(110) Surface to Au Clusters. *J. Phys. Chem. C* **2007**, *111*, 12434–12439.
72. Kruse, N.; Chenakin, S. XPS Characterization of Au/TiO_2 Catalysts: Binding Energy Assessment and Irradiation Effects. *Appl. Catal., A* **2011**, *391*, 367–376.
73. Wang, Z. W.; Wang, X. V.; Zeng, D. Y.; Chen, M. S.; Wan, H. L. Enhance Catalytic Activity for CO Oxidation over Titania Supported Gold Catalysts That Dispersed on SiO_2. *Catal. Today* **2011**, *160*, 144–152.
74. Perdew, J. P.; Burke, K.; Ernzerhof, M. Generalized Gradient Approximation Made Simple. *Phys. Rev. Lett.* **1996**, *77*, 3865–3868.
75. Delley, B. An All-Electron Numerical Method for Solving the Local Density Functional for Polyatomic Molecules. *J. Chem. Phys.* **1990**, *92*, 508–517.
76. Delley, B. From Molecules to Solids with the $DMol^3$ Approach. *J. Chem. Phys.* **2000**, *113*, 7756–7764.
77. Henkelman, G.; Uberuaga, B. P.; Jonsson, H. A Climbing Image Nudged Elastic Band Method for Finding Saddle Points and Minimum Energy Paths. *J. Chem. Phys.* **2000**, *113*, 9901–9904.
78. Henkelman, G.; Jonsson, H. Improved Tangent Estimate in the Nudged Elastic Band Method for Finding Minimum Energy Paths and Saddle Points. *J. Chem. Phys.* **2000**, *113*, 9978–9985.
79. Liu, Z.-P.; Hu, P. Catalytic Role of Gold-Based Catalysts: A Density Functional Theory Study on the CO Oxidation on Gold. *J. Am. Chem. Soc.* **2002**, *124*, 14770–14779.
80. Xie, Y.-P.; Gong, X.-G. First-Principles Studies for CO and O_2 on Gold Nanocluster. *J. Chem. Phys.* **2010**, *132*, 244302.